Supplementary Material

1 SUPPLEMENTARY DATA

In the supplementary material, we present the method used for the error propagation, a table with the statistics of the linear regressions done over the ice flux of each ice tongue (Table S1), the correlation matrix of the different environmental variables used (Figure S1) and an example of the hydrostatic line definition (Figure S2).

1.1 Estimation of the error propagation

There are different sources of error that need to be taken into account. Here we present the calculation of those errors using error propagation. The results are then used as a weight in the ice flux linear regression. First, we need to separate the error bound to the method and the uncertainties integrated into our results due to different processes. There are several processes that can add uncertainty to this methodology, and they are discussed in section 4.3. The errors associated with the method are related to the data collected, the data used and the assumptions made. The total errors for thickness, ice-flux and basal melt were estimated using error propagation from equations 1, 2 and 3 (Drosg, 2009). For the mass-equivalent ice thickness M, we obtained the following error propagation eq (4):

$$\sigma_M = \Big[\big((\frac{-\rho_w}{\rho_w - \sigma i})(h_{sml} - H_a)\big)^2 + \big((\frac{\rho_i}{\rho_i - \sigma w})(h_{sml} - H_a)\big)^2 + \big((\frac{\rho_w \rho i}{\rho_w - \sigma i})(\sigma_{h_{sml}})\big)^2 + \big((\frac{\rho_w \rho i}{\rho_w - \sigma i})(\sigma_{H_a})\big)^2\Big]^{\frac{1}{2}}$$

Where σ_i, σ_w, $\sigma_{h_{sml}}$ and σ_{Ha} are the uncertainties of ice density, water density, height above the ocean surface and firn air content. We used an average value of ice density of 917 +- 5 [kg/mt3] following Griggs and Bamber (2011). Values of water density near the surface and in the vicinity of the Erebus ice tongue have been measured between 1027.94 and 1027.97 kg/mt3 (Stevens et al, 2011), while Han and Lee (2015) use a typical value of 1030 kg/mt3 when calculating thickness at the Campbell Ice Tongue and values close to 1028 kg/mt3 have been found around the Drygalski Ice Tongue (Yoon2020). We decided to use the value of 1028 +- 2 kg/mt3 for the seawater ice density in order to accommodate any possible temporal and spatial variability.

Each ICESat-2 ATL06 height point has an associated error that comes from the propagation due to sampling errors and the first photon bias correction of the land ice algorithm (Smith et al 2019). For the firn air content, we used for each ICESat-2 track and each ice tongue a wider area standard deviation. Then each mass-equivalent thickness (M) error can be converted into metres of ice by dividing σ_M by ρ_i.

The ice flux uncertainties are derived from equation (2), which has three main variables, thickness, velocity perpendicular to the gate and wideness of the gate. We obtained from error propagation the following eq (5):

$$\sigma_\phi = \left[(v_\perp \delta W \sigma_H)^2 + (H \delta W \sigma_{v_\perp})^2 + (v_\perp H \sigma_{\delta W})^2\right]^{\frac{1}{2}}$$

Where σ_H, $\sigma_{v_\perp}$ and $\sigma_{\delta W}$, are the uncertainties for thickness from eq (4), velocity and gate length variability. The HYP3 velocity product obtained from the autoRIFT algorithm has an associated $\bar{v_\epsilon}$ error field (Lei, Gardner and Agram, 2021), we obtained the error at each ICESat-2 point derived thickness. We use the standard deviation of the gate lengths as a measure for errors introduced by the difference that could exist between the velocity field-derived flowlines and the actual glacier flowlines.

We resolve the basal melt uncertainties from the linear model in an analytical form. The results are presented with confidence intervals using the coefficients of average confidence intervals of the flux model as inputs for the flux difference. For Mariner, Borchgrevink and Campbell errors we use the complete propagation method (Equation 6),

$$\sigma_B = \left[(\frac{1}{S}\sigma_\phi)^2 + (\sigma_A)^2\right]^{\frac{1}{2}}$$

accounting for the input errors in the ICESat-2 flux and for the spatial and temporal variability of surface mass balance (mean basal melt values of each ice tongue) over the ice tongue. The estimation of the area (S) between gates is treated as a constant.

2 SUPPLEMENTARY TABLES AND FIGURES

2.1 Figures and Tables

Table S1. Statistics of ice tongue flux linear regressions derived from ICESat-2 measurements. The linear regression models were then used to calculate the basal melt rates of the different ice tongues. Row numbers are related to the numbers of ice tongues in Figure 1. Ice tongues 6, 10 and 11 are excluded from the table as the data and method used to estimate the basal melt differed. The numbers of ice tongues refer to in Figure 1.

	Ice Tongue	r-squared	MSE residuals	RMSE	F-test	Prob(F-test)
1	Erebus	0.064	0.022	0.001	3.48	0.067
2	Nordenskjold	0.152	0.76	0.032	2.33	0.151
3	Harbord	0.926	0.005	0.0007	1210	1.38e-56
4	Cheetham	0.538	0.0033	0.0006	152.8	9.53e-24
5	Drygalski	0.508	1.145	0.389	1041	1.94e-157
7	Tinker	0.126	0.072	0.013	7.377	0.009
8	Aviator	0.730	0.148	0.029	844	6.91e-91
9	Icebreaker	0.281	0.076	0.020	41.84	3.04e-09
12	Tucker	0.964	0.0074	0.002	216.1	04.5e-07

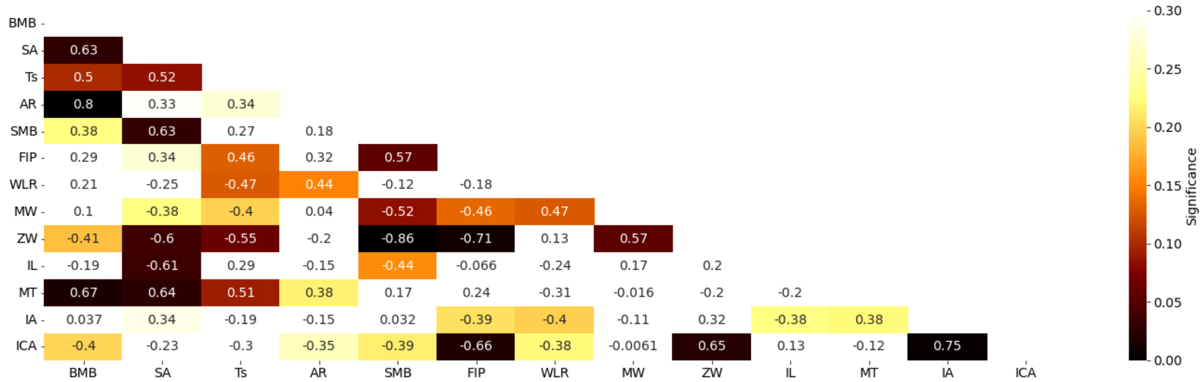

Figure S1. Correlation matrix of the different environmental and geomorphological variables. The variables are snow accumulation (SA), surface temperature (Ts), ice tongue mass turnover (MT), ice tongue to catchment area ratio (AR), surface mass balance (SMB), fast ice persistence (FIP), ice tongue width to length ratio (WLR), meridional wind (MW), ice tongue latitude (IL), ice tongue area (IA), ice tongue basin area (ICA), and zonal wind (ZW). The colour code indicates the significance level of the correlation given by the colour scale from 0 to 0.3. Correlation values are annotated in each cell from -1 to 1.

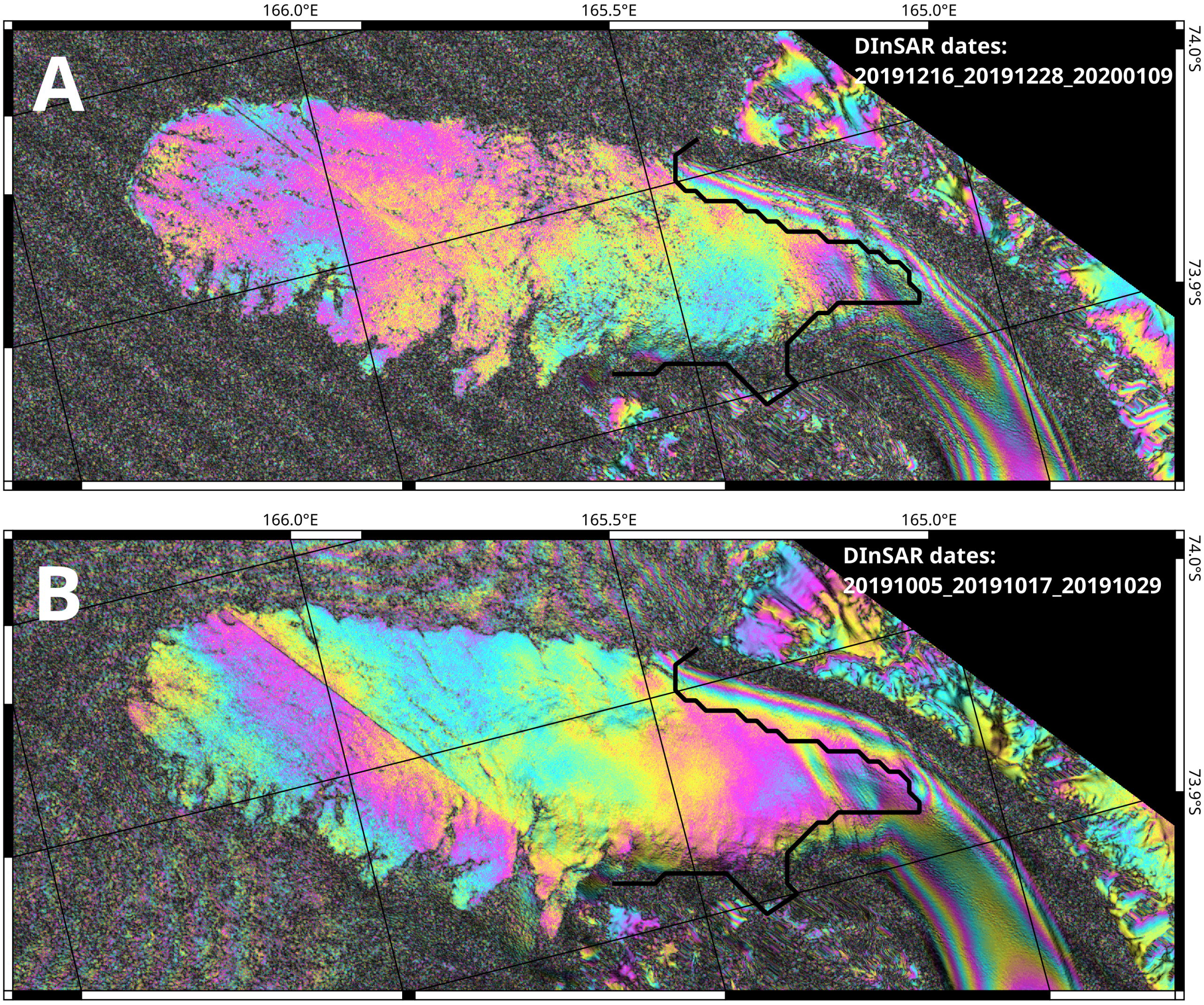

Figure S2. Example over the Aviator Ice Tongue showing the hydrostatic line defined by the alpha maps as a black line and the differential interferograms (DInSAR) observe tidal flexure zone. The alpha map hydrostatic line coincides well with the end of the tidal flexure zone. This is defined by the end of the dense interferometric fringe pattern. The DInSAR maps are created from a pair of InSAR displacement maps, each from a pair of Sentinel-1 SAR images. The dates of the three Sentinel 1 images are A) 16 December 2019, 28 December 2019 and 09 January 2020; B) 05 October 2019, 17 October 2019 and 29 October 2019

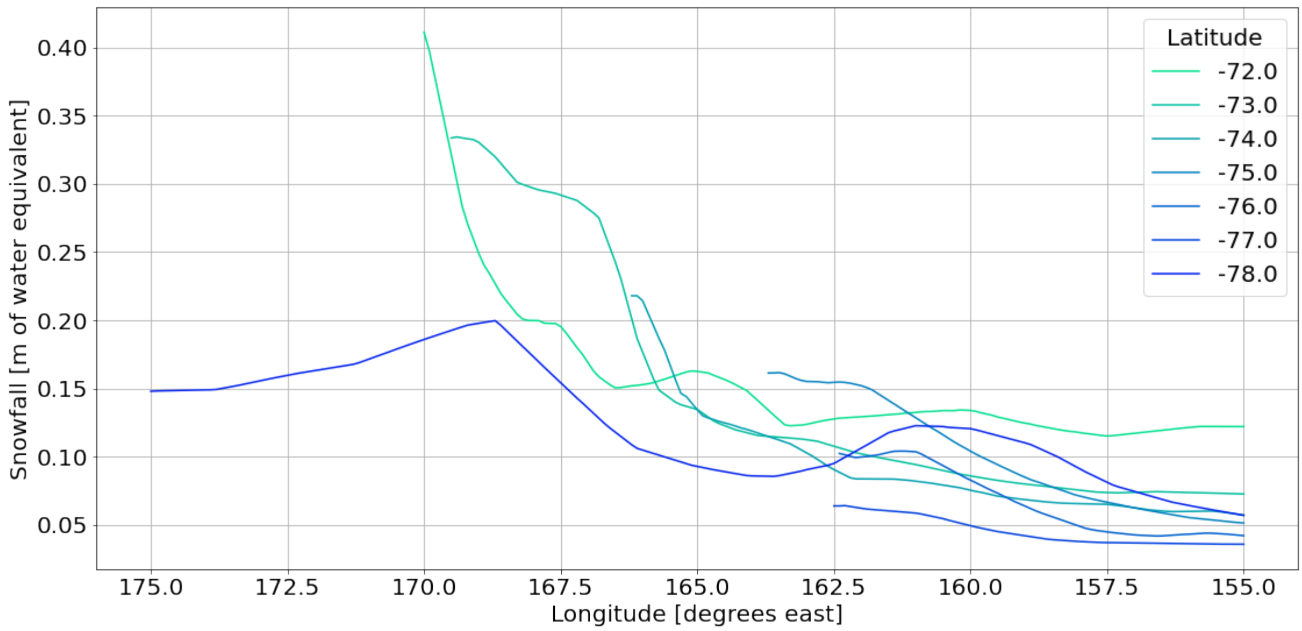

Figure S3. Mean snowfall values from 2000 to 2022 at latitudinal profiles over the Victoria Land Coast based on ERA5-Land at every latitudinal degree between -72 to -78. Each line starts at the coastline and ends inland at 155 degrees Eastern Longitude (inland).